

Paper Number: **1500**

Title: **Bio-like Composite Microstructure Designs for Enhanced Damage Tolerance via Machine Learning**

Authors: Sarah Hankins  
Lars Kothhoff  
Ray S. Fertig, III

## ABSTRACT

Variations of unique and tailored composite microstructures have been observed in nature and have served as templates for the development of new synthetic materials. Microstructures are studied in fish scales for their penetration resistance, in spider webs for energy absorption, and in seashells and bone for their strength and toughness. However, it has proven difficult to reproduce the properties found in natural materials, due to the interaction between the intricate structures at different length scales. Rather than attempting to replicate these materials (biomimetics), the focus of this work is to use a bio-inspired pattern generation algorithm to search for new topologies that outperform traditional composite structures due to their nature-like design. The bio-inspired pattern generation algorithm employed in this research is known as the Gray-Scott model. This model was selected due to its unique ability to manufacture patterns that propagate with time, allowing the reinforcement volume fraction of the composite structure to be controlled. The model is capable of producing Turing patterns, propagating wave fronts, homogeneous oscillations, and chaos. Traditionally, Turing models have been primarily studied for their applications in morphogenesis and pattern development. However, this research extends the application of the Gray-Scott model by investigating the patterns as physical load bearing structures. A methodology was developed by which the patterns can be converted to structures, analyzed for a desired mechanical property, and optimized via Bayesian machine learning algorithms that yield an improvement of the average quality of structures produced by almost a factor of 10.

---

Sarah Hankins <sup>1,3</sup>, Lars Kotthoff <sup>2,3</sup>, and Ray S. Fertig, III <sup>1,3</sup>

<sup>1</sup> Department of Mechanical Engineering, University of Wyoming, Laramie, WY

<sup>2</sup> Department of Computer Science, University of Wyoming, Laramie, WY

<sup>3</sup> Artificially Intelligent Manufacturing (AIM) Center, University of Wyoming, Laramie, WY

## INTRODUCTION

Nature contains a vast array of structures for various applications that have been optimized over millions of years. Evolution removes the weakest links by means of extinction while improving and adapting the top performing structures to meet the needs of the surrounding environment. For example, woodpecker beaks must be able to absorb energy, antlers must be tough, and seed coats must provide penetration resistance. The structures created in nature tend to contain combinations of mechanical properties that are inconceivable in current man-made materials. As a result, materials researchers have turned towards nature as a source of inspiration in a field of study known as biomimetics. This field is dedicated to analyzing and generating bio-inspired structures. As new manufacturing technologies such as 3D printing emerge, the replication of complex configurations such as those found in organic microstructures become attainable [1]. However, mimicking properties found in natural materials is challenging, and in some cases, nearly impossible. This is due in large part to the complex interaction between intricate structures that range in size from molecular to macroscopic [2]. As a result, while natural materials possess optimized properties, the current methods that involve exact replication of these structures are time consuming and often fail to recreate the properties synthetically [1, 2, 3]. Rather than investing time and resources into the study of a single organic structure, the focus of this work is to use a bio-inspired pattern generation algorithm, in conjunction with machine learning algorithms, to search for new biomimetic composite topologies.

The bio-inspired pattern generation algorithm employed in this research is known as the Gray-Scott model. This model was selected due to its unique ability to grow patterns rather than have them instantly appear from random perturbations in the system [4]. Propagating patterns provide control over the reinforcement volume fraction typically encountered in composites. Initially, the model was created to analyze an isothermal system with self-sustaining chemical reactions in a continuously fed, well-stirred, open-tank reactor [5, 6, 7]. However, a study done by Pearson [8] revealed that in two-dimensions the model could generate patterns found in nature. The two-dimensional model utilized Turing's theory that diffusion could cause a steady-state system to become unstable, thereby yielding a pattern [9]. The Gray-Scott model is categorized as a reaction-diffusion model, because two substances are allowed to interact and diffuse with one another [10]. Within the reaction-diffusion category, the model is known as the activation-depletion type, because the concentrations of the two interacting substances oppose one another [11]. The equations governing the change in chemical concentrations due to diffusion are given by

$$\frac{\partial u}{\partial t} = -uv^2 + F(1 - u) + D_u \nabla^2 u \quad (1)$$

$$\frac{\partial v}{\partial t} = uv^2 - (F + k)v + D_v \nabla^2 v \quad (2)$$

where  $u$  and  $v$  are the chemical concentrations,  $D_u$  and  $D_v$  are the diffusion coefficients,  $F$  is the feed rate, and  $k$  is the kill rate [8]. As shown in Equations (1) and (2), chemical V is the activator, because the concentration of chemical V increases when chemical V is present. It can also be shown that chemical U is the substrate, because high concentrations of chemical V reduce the concentration of chemical U [11]. It is assumed that all variables are initially set as positive values. Linear stability analysis on the set of partial differential equations performed by Pearson and Mazin [8, 11] produced a phase diagram for the reaction. Homogeneous oscillations occur around the saddle-node bifurcation curve; Turing patterns, propagating wave fronts, and chaos occur around the Hopf bifurcation curve.

The patterns produced by the Gray-Scott model, to date, have not been converted into structures for mechanical simulation. Prior to this study, the Gray-Scott model has been primarily analyzed in the math and science fields to investigate various integration methods, Laplacian approximations, dynamic systems, and morphogenesis [12, 13, 14, 15, 16]. As a result, in this work we aim to prove that the biomimetic patterns produced by the Gray-Scott model can be transformed into structures that outperform traditional composites due to their nature-like design. Specifically, the target objective is to search for topologies that have an increased damage tolerance.

Damage tolerance refers to the ability of a composite to maintain its strength and integrity even after structural damage has occurred. The main type of structural damage we aim to prevent in this study is crack propagation. The fiber-matrix interface area is a crucial component to arresting cracks in composite structures [17]. As the interfacial area per unit volume increases, so does the amount of energy that can be dissipated [18]. The interfaces act as obstacles that deflect growing cracks, thereby reducing the energy each time one is encountered. As a result, an increase in interfacial area per unit volume tends to correlate to an increase in damage tolerance. Therefore, the bio-like composite structures generated by the Gray-Scott model will be ranked and optimized based on their interfacial area.

## **SIMULATION PROCEDURE**

The two-dimensional Gray-Scott model was implemented in Matlab with the same initial conditions and resolution used by Pearson [8]. As a result, a 2.5 x 2.5 arbitrary unit reaction area was generated with an overlaying 256 x 256 Cartesian grid. A matrix for chemical U and a matrix for chemical V were created to describe the concentration of each chemical across the gridded area. The initial steady-state system was homogeneously filled with chemical U and then perturbed through the addition of chemicals U and V. Prior to any disturbance, the concentration of chemical U was 1 and the concentration of chemical V was 0 across the grid, placing the system in a trivial steady-state environment. A predetermined area in the middle of the grid was then perturbed to a concentration level of 0.5 for chemical U and 0.25 for chemical V. An additional perturbation of  $\pm 1\%$  random noise was added to the system to break the initial square/rectangular symmetry. The system was then allowed to vary with a time step  $t$  of 1 according to the following equations [19, 20].

$$u_{i,j}^{n+1} = u_{i,j}^n + t(-u_{i,j}^n v_{i,j}^{n,2} + F(1 - u_{i,j}^n) + D_u \nabla^2 u_{i,j}^n) \quad (3)$$

$$v_{i,j}^{n+1} = v_{i,j}^n + t(u_{i,j}^n v_{i,j}^{n,2} - (F + k)v_{i,j}^n + D_v \nabla^2 v_{i,j}^n) \quad (4)$$

After each iteration  $n$ , Equations (3) and (4) were used to update the individual matrix values containing the concentrations of chemicals U and V using Euler's Method, periodic boundary conditions, and the five-point finite difference approximation for the 2D Laplacian. The square lattice grid permits  $h = \Delta x = \Delta y = 2.5/256$ , therefore, the Laplacian approximation can be written according to Equation (5) [19, 20].

$$\nabla^2 w_{i,j}^n = \frac{w_{i+1,j}^n + w_{i-1,j}^n + w_{i,j+1}^n + w_{i,j-1}^n - 4w_{i,j}^n}{h^2} \quad (5)$$

To generate different patterns, the feed rate, kill rate, diffusion coefficients, and amount of chemical V added to the system were randomly varied. The feed rate varied from 0 to 0.25 and the kill rate varied from 0 to 0.1 in order to encompass the full pattern generation region described by the reaction-diffusion phase diagram [8, 11]. The diffusion coefficients varied from 0 to  $2 \times 10^{-5}$  according to the maximum diffusion coefficient used by Pearson [8]. Finally, the amount of chemical V added to the system varied from an  $x$  and  $y$  grid length of 0 to 200 (or an area of 0 to 40,000) in the middle of the overlaying 256 x 256 Cartesian grid. The adjustment of these six parameters yields an infinite ensemble of possible outcomes.

Many of the generated patterns have a spatial component and/or a temporal component; the patterns tend to vary with time and/or space. The spatial component was suppressed by limiting the reaction area size to 2.5 x 2.5. To prevent the temporal patterns from evolving infinitely, a reinforcement volume fraction of 30% was implemented; the pattern ceases once it encompasses  $30\% \pm 0.5\%$  of the 2.5 x 2.5 reaction area. Two other types of patterns that are not desirable include patterns that never meet the 30% requirement and homogeneous patterns. In order to bypass these, the evolution of the patterns cease when the concentration profiles no longer change with time or when the number of iterations exceeds 20,000. The patterns that meet the 30% reinforcement volume fraction requirement are converted to structures by analyzing the concentration value of chemical V across the grid according to Equation (6).

$$\begin{aligned} v &\geq \sqrt{F}, & \text{structure (1)} \\ v &< \sqrt{F}, & \text{matrix (0)} \end{aligned} \quad (6)$$

A new matrix, known as the shape matrix, was produced detailing the shape of the structure by assigning a 1 where the concentration of chemical V met the structure requirement and a 0 elsewhere. The requirement for the pattern to be considered a structure comes from a bifurcation diagram produced by Mazin [11] that was a function of the feed rate, kill rate, and concentration of chemical V. According to the diagram, a saddle-node bifurcation curve exists according to the equation  $v = \sqrt{F}$ . Above the curve the system may be stable, whereas below the

curve the system is unstable unless  $v = 0$ . Therefore, since the patterns of interest are primarily stable, they must appear above the saddle-node bifurcation curve.

After the model produces a random structure, a fitness parameter is assigned. The purpose of this parameter is to determine how well the structure will perform in the desired application. As a result, in this study, the fitness parameter ranks the structures in order of damage tolerance. Characterization of the fitness parameter requires prior knowledge of how damage tolerance is increased in traditional composites. The previous section describes how a large interfacial area typically increases the damage tolerance. Therefore, the fitness parameter for this application is a scaled value of the total interfacial area between the structure and the matrix. In order to calculate the fitness parameter, the shape matrix was evaluated. Within the matrix each vertical and horizontal edge that acted as a border between a 1 (structure) and a 0 (matrix) were summed individually. The number of vertical and horizontal edges were then multiplied by the corresponding length of a single mesh element of the  $256 \times 256$  Cartesian grid. Due to the square nature of the grid, the vertical and horizontal edges could be added together and multiplied by a single length to calculate the total interfacial area. The fitness parameter was then calculated by scaling the interfacial area by a factor of 100 in order to obtain values in the range of 0 to 10 as described by Equation (7).

$$FP = \frac{(\# \text{ of edges}) * \left(\frac{2.5}{256}\right)}{100} \quad (7)$$

Within Equation (7),  $FP$  is the fitness parameter,  $\# \text{ of edges}$  is the total number of interfacial borders,  $2.5/256$  is the length of each edge of the single square mesh element, and  $100$  is the scaling factor. A high fitness parameter implies a large interfacial area and a high damage tolerance, while a low fitness parameter implies a small interfacial area and a low damage tolerance. The fitness parameter will also be utilized in conjunction with the machine learning algorithm to aid in the optimization process.

The model generated 225 random structures that met the 30% reinforcement volume fraction requirement and assigned a fitness parameter to each of them. The format of the structures rendered in Figure 1 depicts the chemical representation; where the white portion indicates a high concentration of chemical V, and the black portion indicates a high concentration of chemical U. The shape matrix was then used to convert the chemical representation to a structural representation. In the structural representation, the white portion is the structure and the black portion is the matrix. Eight distinct categories of bio-like structures were produced: spotted, striped, coral, lace, spotted-striped, hexagon, chaotic, and propagating spiral front structures.

Figure 1 illustrates the top performing structures with the highest fitness parameter from each category. The categories were ranked in descending order based on their fitness parameter as follows: 3.96 for lace, 2.00 for spotted, 1.67 for spotted-striped, 1.41 for striped, 0.77 for propagating spiral front, 0.64 for coral, 0.46 for hexagon, and 0.14 for chaotic. As a result, according to the fitness

parameter, the category of structure with the highest damage tolerance was lace while the category of structure with the lowest damage tolerance was chaotic. An additional non-biomimetic category of structure was generated when a bio-like pattern failed to emerge, resulting in an oval structure with a fitness parameter close to zero.

Figure 2 reveals the parameter settings for the randomly generated structures via plots of the feed rate versus kill rate and the diffusion coefficient of chemical V versus the diffusion coefficient of chemical U. The feed rate and kill rate were also plotted against the saddle-node and Hopf bifurcation curves for a general comparison to the results obtained by Pearson [8]. The gray points indicate the parameter settings for the non-biomimetic structures while the colored points indicate the parameter settings for the bio-like structures.

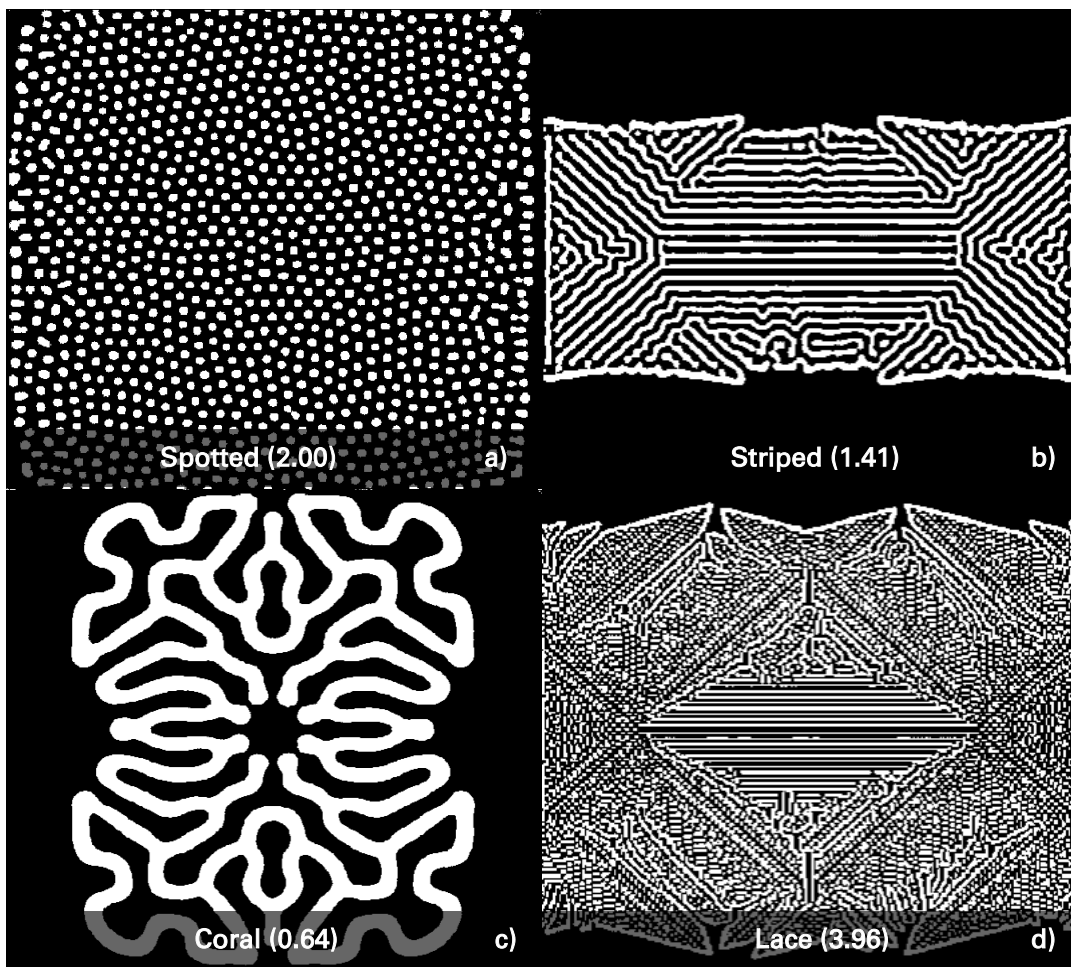


Figure 1. Eight categories of bio-like structures generated by the two-dimensional Gray-Scott model.  
a. spotted structure b. striped structure c. coral structure d. lace structure

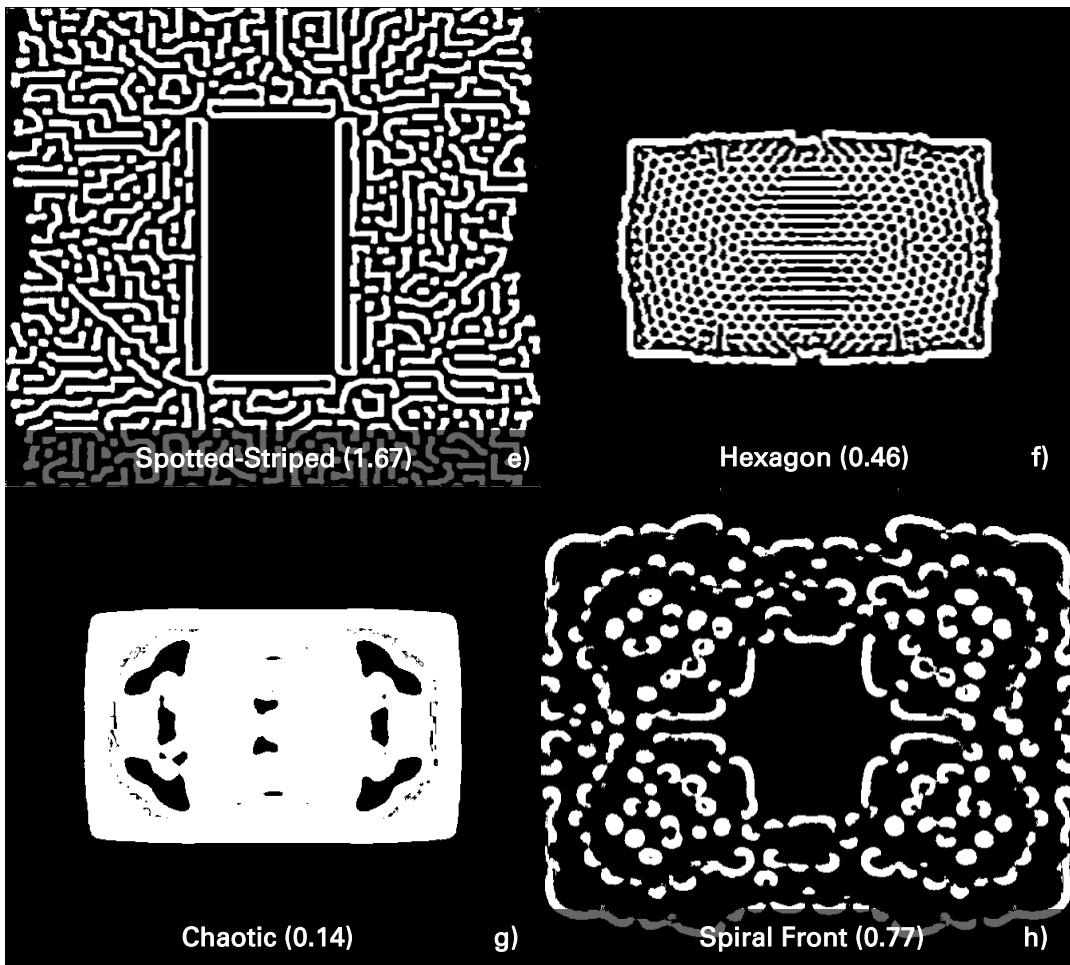


Figure 1. (Continued). e. spotted-striped structure f. hexagon structure g. chaotic structure h. propagating spiral front structure

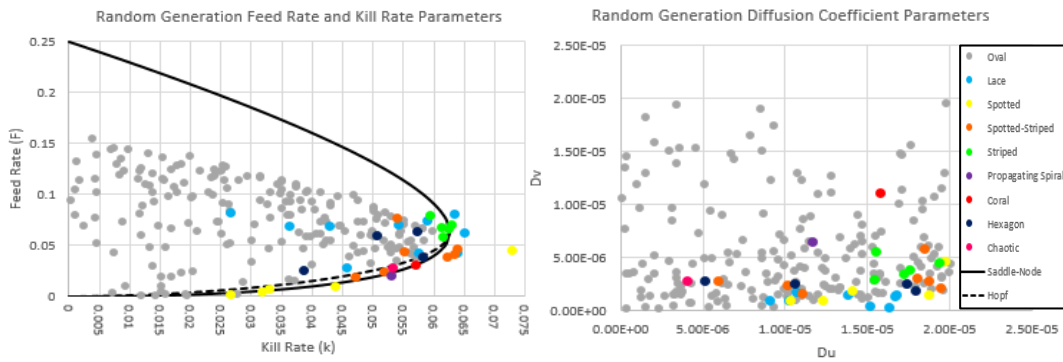


Figure 2. Randomly generated parameters (feed rate, kill rate, and diffusion coefficients).

## MACHINE LEARNING OPTIMIZATION

The purpose of the randomly generated structures was to scope out fitness parameters across the reaction-diffusion search space. The information about the

space was then compiled into a set of training data comprised of the six parameter settings (feed rate, kill rate, diffusion coefficients, and amount of chemical V added to the system) and the fitness parameter for each structure. Next, this information was used to perform numerical optimization via a machine learning method known as Bayesian optimization with a Kriging surrogate model [21]. Bayesian optimization is an iterative process that utilizes a surrogate model and an acquisition function to evaluate the space and guide subsequent searches. The purpose of the surrogate model is to learn about the space from the information provided by the set of training data [22, 23]. The Kriging surrogate model utilizes spatial correlations to minimize the mean error of the weights [24]. The acquisition function is then used to predict a new set of parameters while determining if it should explore the space more or if should exploit an area [22]. For this application, the Bayesian model was trained to maximize the fitness parameter during the optimization procedure based on the set of training data. As a result, the fitness parameter influenced how the algorithm's solutions evolved.

Once the algorithm predicts a new set of parameters, those values get fed back into the Gray-Scott Matlab model to obtain the new structure's fitness parameter. The structure's settings and fitness parameter are then appended to the training data set as a new data entry for the algorithm to learn from. Therefore, each structure generated by the machine learning algorithm is used to aid in the optimization process. In order to ensure that the structures produced by the machine learning algorithm were comparable to the randomly generated structures, the 30% reinforcement volume fraction requirement was enforced. However, in order to ensure a smooth search surface, any structure that had a reinforcement volume fraction less than  $30\% \pm 0.5\%$  was penalized, rather than assigned a fitness parameter of zero. The penalty is described below in Equation (8)

$$FP^* = FP \left( \frac{V_R}{0.3} \right)^p \quad (8)$$

where  $FP^*$  is the new penalized fitness parameter,  $FP$  is the original non-penalized fitness parameter,  $V_R$  is the reinforcement volume fraction,  $0.3$  is the required 30% reinforcement volume fraction, and  $p$  is the penalty. For this application, the penalty was assigned a value of 1 to eradicate any sharp edges on the search surface.

The machine learning algorithm in conjunction with the Gray-Scott model produced 900 new structures. Figure 3 presents the parameter settings for the structures via plots of the feed rate versus kill rate and the diffusion coefficient of chemical V versus the diffusion coefficient of chemical U. The feed rate and kill rate were also plotted against the saddle-node and Hopf bifurcation curves for a general comparison to the results obtained by Pearson [8]. The gray points indicate the parameter settings for the random generation, while the red points indicate the parameter settings generated by the machine learning algorithm. The parameter settings reveal how the machine learning algorithm explored and exploited the space. The areas with clusters of red points expose where the machine learning algorithm determined it could produce the most damage tolerant structures. The remaining individual red points indicate where the machine learning algorithm explored the search space but failed to find structures with a high damage tolerance.

The majority of the structures generated either met the 30% reinforcement volume fraction requirement or were homogeneous; resulting in only 5.2% of the structures being penalized. Of the 900 structures generated, 78.2% were lace, 18.1% were homogeneous, 3% were oval, 0.4% were spotted, and 0.2% were coral. As a result, the machine learning algorithm determined that the category of structure with the highest damage tolerance was lace; the top four structures are displayed in Figure 4a-d. A close examination of the top four structures reveals intricate features with an absence of perfect symmetry. In nature, most structures are not uniform and contain multitudes of imperfections. Research has revealed that the imperfections tend to be a result of structural adaptation from the forces applied by the surrounding environment. Therefore, it has been discovered that the defects tend to improve the mechanical properties of biological structures [25]. A similar phenomenon can be shown in the structures generated by the machine learning algorithm. Figure 4e presents a structure that was generated with near perfect symmetry. While the structure looks similar to the top four, its symmetry reduces the fitness parameter by 19.5%.

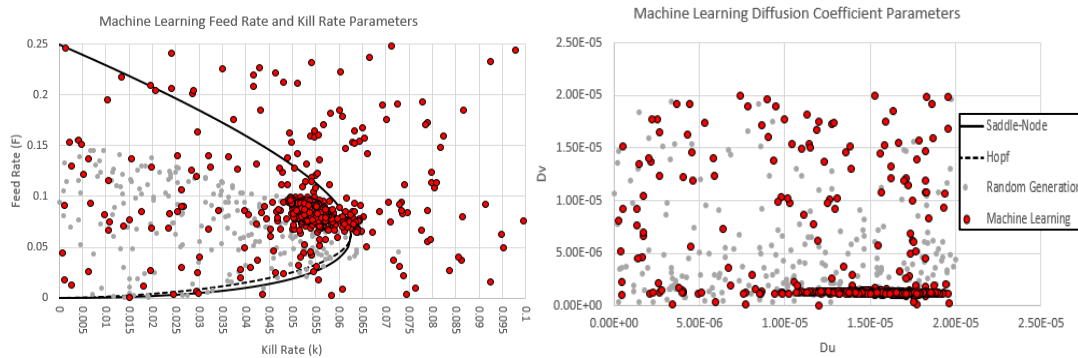


Figure 3. Parameter settings (feed rate, kill rate, and diffusion coefficients) generated by the machine learning algorithm.

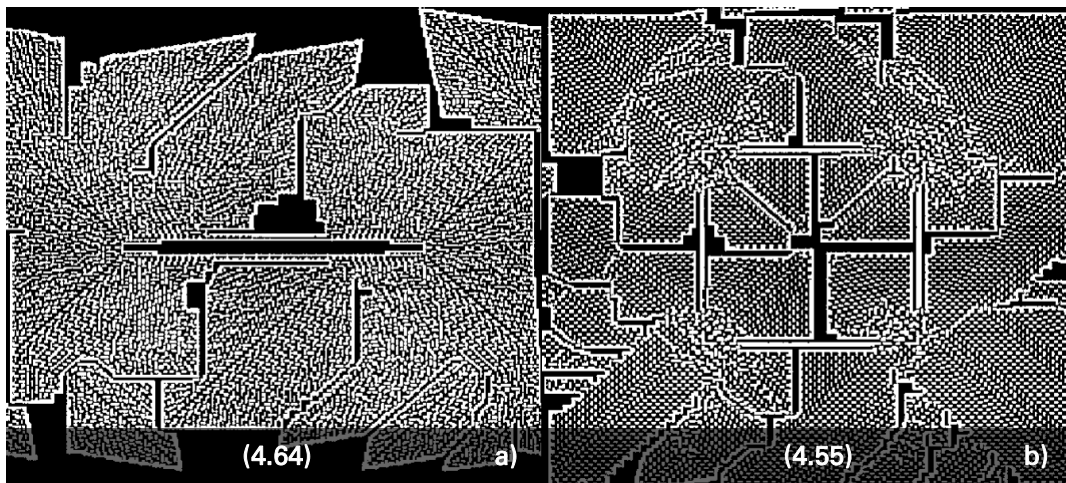


Figure 4. Structures generated by the machine learning algorithm with their corresponding fitness parameter enclosed in parenthesis. a-d. top four structures with the highest damage tolerance

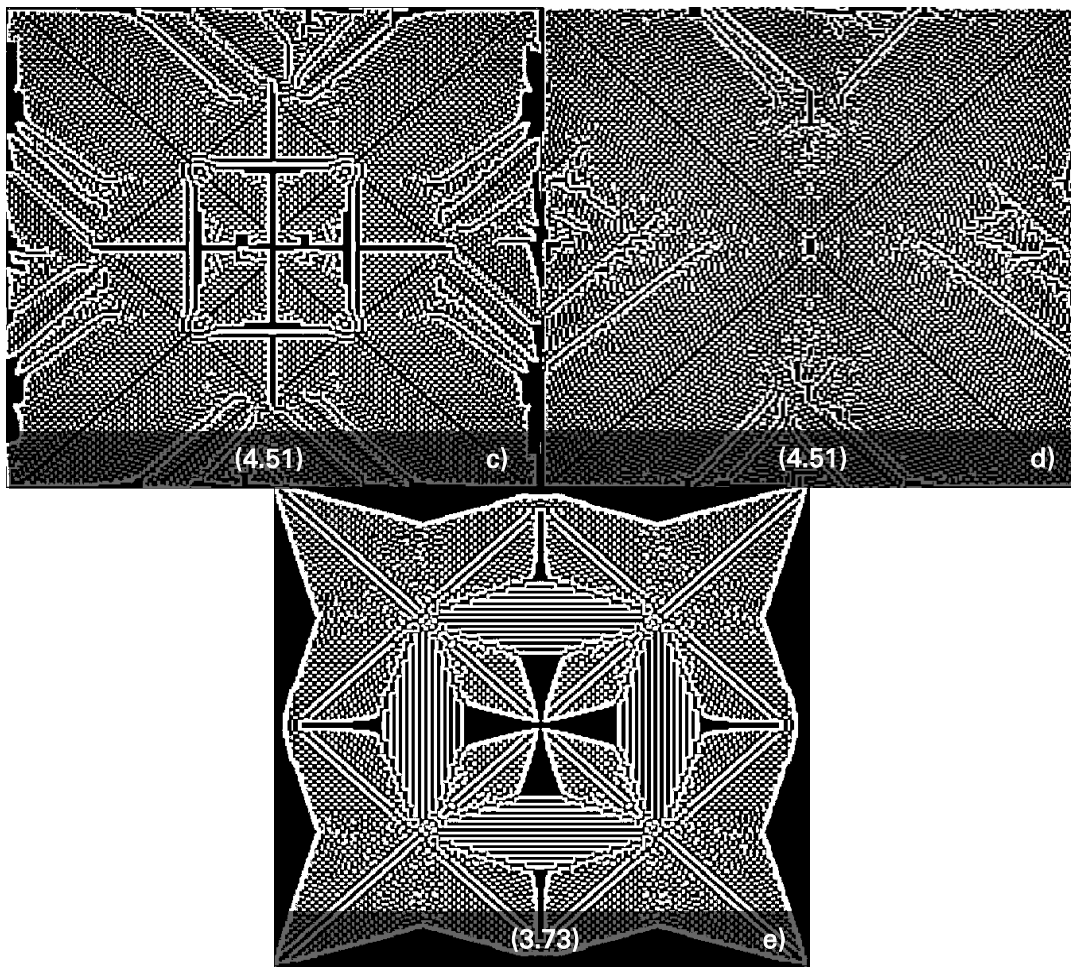


Figure 4. (Continued). a-d. top four structures with the highest damage tolerance  
 e. symmetric structure

## RESULTS

The orange box and whisker plot in Figure 5 displays the fitness parameters for the 225 randomly generated structures. The majority of the structures had a fitness parameter close to zero, because a bio-like pattern was unable to emerge resulting in an oval structure with a small interfacial area per unit volume. The average fitness parameter, indicated by the x marker, for the randomly generated structures was 0.31 and the maximum fitness parameter was 3.96. Due to the majority of the structures exhibiting near zero fitness parameters, any structure with a fitness parameter higher than the average was considered an outlier. The blue box and whisker plot in Figure 5 displays the fitness parameters for the 900 machine learning generated structures. A portion of the structures had a fitness parameter of zero because they were homogeneous. The average fitness parameter, indicated by the x marker, for the machine learning generated structures was 2.98 and the maximum fitness parameter was 4.64. Since the majority of the structures generated

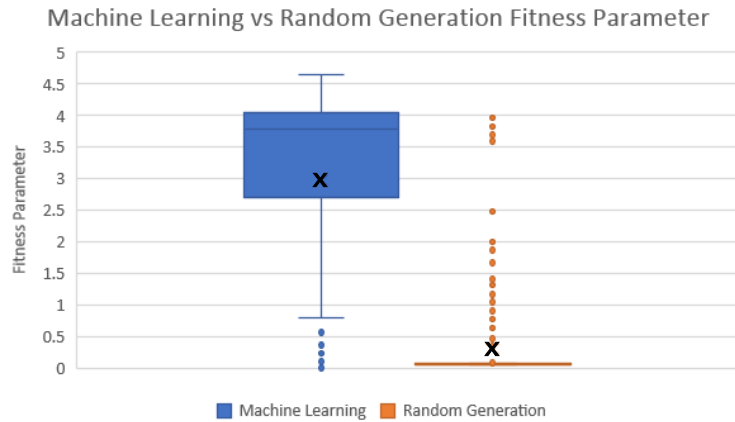


Figure 5. Box and whisker plots for the fitness parameters obtained from the randomly generated structures (orange box) and machine learning structures (blue box).

by the machine learning algorithm had a high fitness parameter, any structure with a fitness parameter near zero was considered an outlier. As a result, the numerical optimization performed by the machine learning algorithm was able to increase the average fitness parameter by nearly a factor of 10, exceed the maximum randomly generated fitness parameter, and produce an augmented quantity of structures with elevated fitness parameters. Therefore, the machine learning algorithm in conjunction with the two-dimensional Gray-Scott model maximized the interfacial area for a fixed 30% reinforcement volume fraction, leading to an increase in damage tolerance for the bio-like structures.

In addition to generating more damage tolerant structures, the machine learning algorithm was also able to speed up the pattern generation process by a factor of 2.16. The computational time required for the randomly generated structures, that met the 30% reinforcement volume fraction requirement, was 4,619 minutes or approximately 20.53 minutes per structure. The computational time required for the machine learning generated structures, that met the 30% reinforcement volume fraction requirement, was 6,547 minutes or approximately 9.49 minutes per structure. The random generation required more time to produce structures, because a majority of the parameter settings resulted in homogeneous patterns. Therefore, a lot of time was spent analyzing random parameter settings that did not produce bio-like structures. However, the machine learning algorithm required less time to yield structures, because it was able to evaluate the search space and provide optimized parameter settings that would likely produce a bio-like structure. As a result, the machine learning algorithm provided a method by which parameter settings could be optimized for a desired mechanical property and reinforcement volume fraction while decreasing the computational time.

## CONCLUSION

Prior to this study, there has been no mechanical analysis performed on the patterns produced by the Gray-Scott model. Therefore, the results revealed a

methodology by which a collection of bio-inspired composite topologies generated by the Gray-Scott model can be converted to structures that meet a fixed reinforcement volume fraction, analyzed for a desired mechanical property, and optimized via machine learning algorithms. Without the implementation of the model-based Bayesian machine learning optimization, it is difficult to produce a large quantity of high quality bio-like structures. While random generation of the parameter settings provides an unbiased search of the reaction space, a majority of the settings produce non-biomimetic structures. However, the random generation provides an excellent set of training data for the machine learning algorithms to learn from. As a result, the model-based Bayesian machine learning optimization is able to learn about the search space quickly and effectively, yielding an improvement of the average fitness parameter by almost a factor of 10 over the randomly generated structures. Therefore, the machine learning algorithms significantly increase the quality of structures produced.

Future work involves using the model to generate three-dimensional structures with mechanical properties that can be analyzed through realistic loading configurations in Abaqus. The end goal is to create application specific bio-like designs that can be fabricated using additive manufacturing techniques.

## REFERENCES

1. Y. Yang, X. Song, X. Li, Z. Chen, C. Zhou, Q. Zhou and Y. Chen, "Recent Progress in Biomimetic Additive Manufacturing Technology: From Materials to Functional Structures," *Advanced Materials*, no. 1706539, pp. 1-34, 2018.
2. U. G. Wegst, H. Bai, E. Saiz, A. P. Tomsia and R. O. Ritchie, "Bioinspired structural materials," *Nature Materials*, vol. 14, pp. 23-36, 2015.
3. O. A. Oguntona and C. O. Aigbavboa, "Barriers hindering biomimicry adoption and application in the construction industry," *African Journal of Science, Technology, Innovation and Development*, vol. 11, no. 3, pp. 289-297, 2019.
4. K. J. Lee, W. D. McCormick, Q. Ouyang and H. L. Swinney, "Pattern Formation by Interacting Chemical Fronts," *Science*, vol. 261, no. 5118, pp. 192-194, 1993.
5. P. Gray and S. K. Scott, "AUTOCATALYTIC REACTIONS IN THE ISOTHERMAL, CONTINUOUS STIRRED TANK REACTOR ISOLAS AND OTHER FORMS OF MULTISTABILITY," *Chemical Engineering Science*, vol. 38, no. 1, pp. 29-43, 1983.
6. P. Gray and S. K. Scott, "Sustained Oscillations and Other Exotic Patterns of Behavior in Isothermal Reactions," *Journal of Physical Chemistry*, vol. 89, pp. 22-32, 1985.
7. P. Gray and S. Scott, "Autocatalytic reactions in the isothermal, continuous stirred tank reactor," *Chemical Engineering Science*, vol. 39, no. 6, pp. 1087-1097, 1984.
8. J. E. Pearson, "Complex Patterns in a Simple System," *Science*, vol. 261, no. 5118, pp. 189-192, 1993.
9. A. M. Turing, "The Chemical Basis of Morphogenesis," *Biological Sciences*, vol. 237, no. 641, pp. 37-72, 1952.
10. S. Kondo and T. Miura, "Reaction-diffusion model as a framework for understanding biological pattern formation," *Science*, vol. 329, pp. 1616-1620, 2010.
11. W. Mazin, K. E. Rasmussen, E. Mosekilde, P. Borckmans and G. Dewel, "Pattern formation in the bistable Gray-Scott model," *Mathematics and Computers in Simulation*, vol. 40, pp. 371-396, 1996.
12. T. Wang, F. Song, H. Wang and G. E. Karniadakis, "Fractional Gray-Scott model: Well-posedness, discretization, and simulations," *Computer Methods in Applied Mechanics and Engineering*, vol. 347, pp. 1030-1049, 2019.
13. A. Giri and S. Kar, "Unraveling the diverse nature of electric field induced spatial pattern formation in Gray-Scott model," *Journal of Chemical Physics*, vol. 150, no. 9, 7 3 2019.
14. H. TAKAGI and K. KANEKO, "PATTERN DYNAMICS OF A MULTI-COMPONENT REACTION-DIFFUSION SYSTEM: DIFFERENTIATION OF REPLICATING SPOTS," *International Journal of Bifurcation and Chaos*, vol. 12, no. 11, pp. 2579-2598, 19 12 2002.
15. Y. N. Kyrychko, K. B. Blyuss, S. J. Hogan and E. Schöll, "Control of spatiotemporal patterns in the Gray-Scott model," *Chaos*, vol. 19, no. 4, 2009.
16. A. Adamatzky, "Generative complexity of Gray-Scott model," *Communications in Nonlinear Science and Numerical Simulation*, vol. 56, pp. 457-466, 2018.
17. P. Ladeveze, E. Baranger, M. Genet and C. Cluzel, *Ceramic Matrix Composites: Materials, Modeling and Technology*, Wiley, 2014, pp. 528-531.
18. W. Gu, H. F. Wu, S. L. Kampe and G. Q. Lu, "Volume fraction effects on interfacial adhesion strength of glass-fiber-reinforced polymer composites," *Materials Science and Engineering A*, vol. 277, no. 1-2, pp. 237-243, 31 1 2000.
19. W. Wang, Y. Lin, F. Yang, L. Zhang and Y. Tan, "Numerical study of pattern formation in an extended Gray-Scott model," *Communications in Nonlinear Science and Numerical Simulation*, vol. 16, no. 4, pp. 2016-2026, 1 4 2011.

20. A. MUNTEANU and R. V. SOLÉ, "PATTERN FORMATION IN NOISY SELF-REPLICATING SPOTS," *International Journal of Bifurcation and Chaos*, vol. 16, no. 12, pp. 3679-3685, 23 2 2007.
21. B. Bischl, J. Richter, J. Bossek, D. Horn, J. Thomas and M. Lang, "mlrMBO: A Modular Framework for Model-Based Optimization of Expensive Black-Box Functions," 9 3 2017.
22. M. Feurer and F. Hutter, "Hyperparameter Optimization," in *Automated Machine Learning: Methods, Systems, Challenges*, Springer, 2018, pp. 3-33.
23. D. R. Jones, M. Schonlau and W. J. Welch, "Efficient Global Optimization of Expensive Black-Box Functions," *Journal of Global Optimization*, vol. 13, no. 4, pp. 455-492, 1998.
24. S. Sakata, F. Ashida and M. Zako, "Structural optimization using Kriging approximation," *Computer Methods in Applied Mechanics and Engineering*, vol. 192, no. 7-8, pp. 923-939, 14 2 2003.
25. D. Jiao, Z. Liu, Z. Zhang and Z. Zhang, "Intrinsic hierarchical structural imperfections in a natural ceramic of bivalve shell with distinctly graded properties," *Scientific Reports*, vol. 5, pp. 1-13, 22 7 2015.